On the Use of Recycled PVB to Develop Sustainable Separators for Greener Li-Ion Batteries

ADVANCED SUSTAINABLE SYSTEMS
www.advsustainsys.com

On the Use of Recycled PVB to Develop Sustainable Separators for Greener Li-Ion Batteries

Silvia Porporato, Hamideh Darjazi, Matteo Gastaldi, Alessandro Piovano, Angelica Perez, Beatriz Yécora, Alberto Fina, Giuseppina Meligrana, Giuseppe A. Elia, and Claudio Gerbaldi**

In this work, sustainable Li-based battery separators are prepared starting from a waste material from the glass industry, *viz.* polyvinyl butyral (PVB) widely used as a sacrificial interlayer in high impact-resistant windows. First, polymeric membranes are prepared via the phase-inversion method using commercial PVB as the backbone and 4,4′-methylenebis (cyclohexylisocyanate) as a crosslinking agent. They are characterized from a physicochemical viewpoint by thermomechanical analysis, infrared spectroscopy, and scanning electron microscopy, and are successfully tested as separators in Li-metal cells with LP30 electrolyte. Electrical and electrochemical properties are evaluated by impedance spectroscopy and galvanostatic cycling, providing comparable results with commercial Celgard 25 µm monolayer microporous polypropylene separator. As a proof-of-concept, for the first time, recycled PVB-based polymer membranes from wasted car glasses are prepared, adjusting the synthesis protocol to account for the presence of plasticizers and contaminants. They show a dense elastomeric appearance and proved to be compatible with Li metal and stable upon 600 h of Li plating/stripping. The electrochemical window is compatible with the $LiFePO_4$ cathode, as demonstrated by prolonged galvanostatic cycling (250 cycles) in laboratory-scale cells. Preliminary results are highly encouraging and pave the way to developing novel separators for safe, low-cost, and sustainable energy storage devices.

1. Introduction

Nowadays, most of the world energy supply derives from fossil fuels, which knowingly present serious issues related to depletion of limited natural resources, pollution, development of greenhouse gases, and consequently climate changes.[1] On these bases, humankind needs to generate and store energy sustainably and efficiently, moving from non-renewable to renewable resources and combining them with adequate energy storage systems (ESSs).[2,3] Indeed, the adoption of renewables is challenged by their intermittency and the incapacity to cope with demand fluctuations, particularly when implemented in urban grids. For these reasons, ESSs are essential to couple energy generation and distribution.[4] In fact, they find applications in various sectors, spanning from automotive to personal devices and residential plants.[3] Given the wide variety of applications, each ESS requires tailor-made features, and thus, the chemistry behind all these devices can differ significantly.

S. Porporato, H. Darjazi, M. Gastaldi, A. Piovano, G. Meligrana, G. A. Elia, C. Gerbaldi
GAME Lab
Department of Applied Science and Technology (DISAT)
Politecnico di Torino
Corso Duca Degli Abruzzi 24, Turin 10129, Italy
E-mail: alessandro_piovano@polito.it; claudio.gerbaldi@polito.it

The ORCID identification number(s) for the author(s) of this article can be found under https://doi.org/10.1002/adsu.202400569

DOI: 10.1002/adsu.202400569

S. Porporato, H. Darjazi, M. Gastaldi, A. Piovano, G. Meligrana, G. A. Elia, C. Gerbaldi
National Reference Centre for Electrochemical Energy Storage (GISEL)—INSTM
Via G. Giusti 9, Florence 50121, Italy

A. Perez, B. Yécora
LUREDERRA Technological Centre
Perguita Industrial Area
Los Arcos 31210, Spain

A. Fina
Department of Applied Science and Technology (DISAT)
Politecnico di Torino
Viale Teresa Michel 5, Alessandria 15121, Italy

Lithium-ion batteries (LIBs) are at the moment the leading technology in the market of electric vehicles and portable electronic devices, basically thanks to their unparalleled energy density, coulombic efficiency, low weight, fast charge/discharge, and long lifetime.[5,6] Each battery consists of three major components: two physically separated electrodes (the cathode and the anode) and the electrolyte, which enables the ions transfer (thus balancing the reactions at the electrodes). Once the electrodes are connected externally, the circuit is closed, and chemical reactions proceed at both electrodes, thus liberating electrons that flow in the external circuit.[7] Over the years, research aimed to study and implement each component in order to improve performance in terms of energy and power density, electrochemical stability, and cyclability.

Electrolytes are mainly divided into three categories: liquid electrolytes,[8–10] gel-polymer electrolytes,[11,12] and solid-state electrolytes.[13,14] Currently, liquid electrolytes are the most widely used technology, consisting basically of a salt dissolved into a solvent. In order to mechanically and physically isolate the two electrodes, thus avoiding short-circuit, a solid barrier, namely the separator, is used, which is soaked into the liquid electrolyte. Its role is essential since it is responsible for the overall safety of batteries. While isolating the opposite poles, it must be permeable to ionic flow, allowing rapid ion transport back and forth. Another crucial aspect is its ability to work as an electric insulator, thereby minimizing any processes that might negatively impact the electrochemical energy efficiency of the battery.[15]

Over the years, a wide range of separators has been used in ESSs, made of various materials, including cellulose, cellophane, polyolefins, nonwoven fabrics, glass fibers, foams, and other synthetic polymeric materials. As battery technology has advanced, the role of separators has become increasingly complex and challenging,[16] accounting for a relevant portion of the total cost of LIBs.[17] In this context, we hereafter propose the profitable production of a separator based on polyvinyl butyral (PVB), which is typically used as a sacrificial interlayer in high-impact-resistant windows: as a result, we convert a potential waste material into a high-added-value product.

PVB is a random terpolymer obtained from vinyl butyral (≈80%), vinyl alcohol (≈18–24%), and vinyl acetate (≈1–4%) as monomers.[18] The random structure of PVB results in an amorphous polymer with excellent optical transparency, adhesive properties, hardness, and flexibility. From a technological perspective, it is primarily utilized as a raw material for manufacturing laminated safety glass sheets in the automotive industry (such as windshields, side and roof glasses)[19] and in architecture (windows, structural glazing, roofs/floors, staircases and beams).[20] The hydroxyl groups of vinyl alcohol are able to form hydrogen and covalent bonds to the surface of polar substrates and, thus, are accountable for the adhesion of the PVB interlayer–glass interface in the lamination process.

Unplasticized vinyl acetal polymers are rigid and inflexible, presenting processing challenges. To overcome this issue, PVB is mixed with compatible plasticizers, thereby decreasing the polymer glass transition temperature (T_g), resulting in enhanced flexibility and ductility even at room temperature. Currently, phthalate-free plasticizers are employed for PVB plasticization, such as triethyleneglycol di-(2-ethyl hexanoate) or tetraethylene glycol di-n-heptanoate (TEGH), dibutyl sebacate (DBS), dihexyl adipate (DHA), dioctyl adipate (DOA), hexyl cyclohexyl adipate, or combinations of heptyl and nonyl adipates.[21,22] Applications of PVB include the manufacture of glasses for the photovoltaic industry[23,24] and its use as a binder in enamels, inks, and adhesives.[25] The global market for PVB films is expected to experience significant growth in the upcoming years, driven by the increasing industrialization and urbanization trends.[26] Nevertheless, the glass industry requires precise and stringent specifications for raw PVB materials; consequently, preference is often given to virgin PVB due to its superior quality.[27] The use of recycled PVB could potentially address the issues related to the increasing demand, even though, at the moment, a recycling procedure of PVB is not fully defined at an industrial scale.[27–29] This is primarily due to decreased optical properties during recycling and the unavoidable presence of many contaminants. Thus, the post-consume PVB fraction lacking optical and mechanical requirements for its original purpose is incinerated or landfilled, causing tons of losses every year, even though it could find a second life in various scenarios.[30]

PVB can be used as a starting reagent to obtain a wide range of high-value technological materials, owing to the presence of different reactive groups, especially the —OH groups that can undergo condensation reactions.[31] For instance, in combination with diisocyanates, the hydroxyl groups of PVB react in a condensation reaction, giving repeating urethane linkages (polyurethane). Successively, the establishment of intermolecular hydrogen bonds and the amide tautomerisation through the backbone allow for the production of high-performance materials.[32,33] The brilliant mechanical features come from the divergent nature of polyols and isocyanates: the former possess long chains that provide flexibility and represent soft segments, while the latter are often short-chain molecules with a higher degree of crystallization, resulting in hard and tightly packed segments. This segments mixture confers to polyurethane materials high adaptability and renders them successful in a wide range of applications, among which also battery separators.[34–38] However, only in two articles those polyurethane separators were actually produced from PVB, and only from pristine PVB,[39,40] making the whole process economically unfeasible with respect to other cheaper materials, despite the innovative tunability of the chemical process.

In this work, we prepared PVB-derived polymer membranes to be used as separators in Li-based batteries. We developed an easy and scalable procedure, based on the reaction between sustainably sourced PVB with a diisocyanate, which results in a polyurethane membrane with controllable and reproducible porosity. After the preparation, the membranes were characterized from the physicochemical point of view through infrared spectroscopy (IR), thermogravimetric analysis (TGA), differential scanning calorimetry (DSC), dynamic mechanical analysis (DMA) and field-emission scanning electron microscopy (FE-SEM). Successively, they were tested as separators in lab-scale Li-metal cells after soaking in 1M $LiPF_6$ 1:1 v/v EC-DMC (LP30) as the electrolyte, comparing the obtained results with commercial polymeric Celgard®2400 monolayer polypropylene separator. The soaking properties, ionic conductivity, electrochemical stability, and galvanostatic and potentiostatic cycling were evaluated, to demonstrate the practical application in lab-scale cells. After promising results were obtained with commercial PVB, new

membrane separators were also prepared, for the first time to our knowledge, from the recycled PVB that was derived from automotive glasses waste by our partners within the framework of the H2020 European project "*SUNRISE*". The project is developing an innovative optical multi-sensor sorting tool to classify the laminated glasses according to the composition and degradation of the PVB layer. Sorted PVB that lacks optical and mechanical requirements for its original purpose, is repurposed for a second life in other fields, such as, in the present case, high added value products in the energy storage field. In this respect, the great novelty of this work relies on the possibility of providing a new life to waste material and promoting a virtuous, sustainable management of resources in a circular economy perspective.

2. Experimental Section

2.1. Materials

Commercial PVB (structure depicted in Figure S1 - Supporting Information, CAS 63148-65-2) was purchased from Sigma-Aldrich and used as received. Its M_w was determined by Gel Permeation Chromatography (GPC) using DMF as solvent and 0.05 M LiBr as mobile phase. The sample had a 3 mg mL^{-1} concentration. Results showed M_W = 135600 g mol^{-1} and M_{WD} = 8.6 (Figure S2, Supporting Information). Chloroform (CAS 67-66-3, purity ≥ 99.5%), and *N*-*N*-dimethylpyrrolidone (NMP, CAS 872-50-4, purity ≥ 99.0%) were obtained from Merck and used without further purification. 4,4′-methylenebis(cyclohexyl isocyanate) (H_{12}MDI, CAS 5124-30-1, purity ≥ 88.0%) was provided by Sigma-Aldrich and used as received. Recycled PVB was obtained from Lurederra Technological Center (Los Arcos, Spain), within the frame of the H2020 European project *SUNRISE*, and was obtained by a mechanochemical process, involving shredding, sieving, and chemical treatment via acid cleaning, basic stabilization and water washing in sequential steps.[41] $LiFePO_4$ (LFP) was purchased from Sigma-Aldrich (battery grade, with a declared capacity of ca. 170 mAh g^{-1}), as well as the lithium hexafluorophosphate electrolyte solution (1M $LiPF_6$ 1:1 v/v EC and DMC, battery grade); the electrolyte solution (hereafter referred to as LP30) was stored in an Ar-filled dry glovebox (H_2O and O_2 < 0.5 ppm). Conductive carbon C65 (Imerys, 80 wt.%) and polyvinylidene fluoride (PVdF, Solef 6020, Solvay, 20 wt.%) were obtained and used without further purifications. Celgard® 2400 monolayer microporous polypropylene (PP, 25 µm thick) membrane was used as a benchmark separator in this study.

2.2. Hydroxyl Group Calibration

The quantity of hydroxyl group in PVB was determined by IR spectroscopy,[42] preparing a calibration curve with 2-ethylhexan-1-ol in chloroform and measuring in the same conditions two solutions of PVB dissolved in chloroform (with known mass/volume concentrations). The solutions were measured with a Bruker Vertex70 FT-IR spectrophotometer within a liquid cell, equipped with two KBr windows spaced at ca. 200 µm. Such spectroscopic analysis, shown in Figure S3 (Supporting Information), resulted in an average —OH concentration of 0.0172 mol g^{-1} of PVB, in line with what was reported by Lian et al. for commercial PVB.[39]

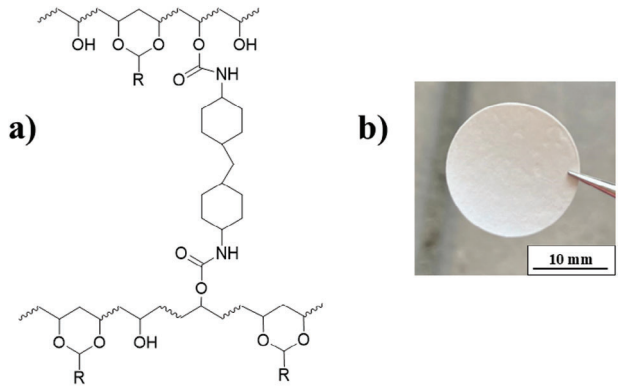

Figure 1. a) Schematic structure of the obtained polymer network, b) digital photograph of the membrane after drying.

2.3. PVB-Based Membrane Preparation

The preparation of the PVB-based polymer membranes is based on a phase inversion technique, known as a coagulation bath.[39,40,43] PVB was dissolved in NMP (PVB:NMP = 1:15, m/m) and kept under continuous stirring for 2 h, in order to obtain a clear and homogenous solution. Successively, H_{12}MDI (PVB:H_{12}MDI = 5:1, m/m) was added under stirring for 30 min at 70 °C. Finally, deionized water (PVB:H_2O = 1:1, m/m), acting as the nonsolvent, was added to precipitate white micelles, which were continuously stirred until dissolution. Thus, the solution became viscous and slightly turbid. The obtained slurry was coated onto a glass plate using a doctor blade with a gap of 500 µm, followed by immersion into a water bath to precipitate the polymer membrane. The polymeric structure of the membrane is sketched in **Figure 1a**. Different proportions of solvent and nonsolvent in the coagulation bath can lead to membranes with different morphologies: porous membranes were obtained using a water-based coagulation bath, while dense membranes were obtained using NMP–water mixture (NMP:H_2O = 1:10, v/v). In both cases, after 1-h bath, the resulting membranes were washed with excess deionized water and dried under vacuum at 40 °C for 24 h. Afterward, membranes were punched into self-standing disks (Figure 1b), ready to be soaked with the electrolyte, and used as separators inside electrochemical cells. The resulting thickness of the membranes is 100 µm (±10 µm).

Polymer membranes from recycled PVB (rePVB) were also manufactured. The preparation resulted in being less straightforward compared to the previous one, due to the presence of plasticizers (added to improve the elasticity and processability of the material) and impurities (due to prolonged uses under all possible weather conditions). Particularly, accordingly to recent quantitative analysis, the weight ratio between polymers and plasticizers is roughly 1:1.[44] Therefore, the rePVB:H_{12}MDI ratio was reduced to 20:1, not only to account for the effective lower amount of polymer in the material but also to compensate for the stickiness induced by the plasticizers in the slurry. Since the addition of H_{12}MDI immediately made the solution more viscous even at room temperature, the solution was first spread in a glass Petri dish, then heated at 70 °C (the same temperature as for the preparation of the membranes with pure, commercial PVB), and finally directly immersed into the coagulation bath,

constituted only by water. This simplified procedure did not allow for a fine control of morphology and thickness (≈150 µm) of the membranes, but it was necessary to enable the use of a highly contaminated raw material as rePVB. In this case, there is no distinction between porous and dense membranes since just one type of coagulation bath was used.

2.4. Characterisation Techniques

Scanning electron microscopy (SEM) secondary electrons contrast images were collected with 5 keV electrons using an in-lens detector of a Zeiss SUPRA 40 (Zeiss SMT, Oberkochen, Germany) field emission electron microscope (FESEM). A metallization step with a few nm thick Pt layer was needed before the FESEM analysis to avoid the samples' charging. IR spectra were acquired in ATR mode with a Bruker Vertex70 FT-IR spectrophotometer, equipped with an MCT detector, at a resolution of 2 cm^{-1}. Pure samples were deposited on a diamond crystal. The intensity of the spectra was normalized with respect to the intensity of the fingerprints of the PVB backbone. The thermal resistance was measured by thermogravimetric analysis (TGA, Netzsch TG 209 F3). The analysis was conducted between 25 and 800 °C under a nitrogen atmosphere (N_2 flux of 100 mL min^{-1}), using a heating ramp of 10 °C min^{-1}. Differential scanning calorimetry (DSC, Netzsch 214 Polyma Equipment) was carried out to evaluate the glass transition temperature (T_g). The measurements were conducted in a temperature range between −50 and 100 °C with a heating rate of 10 °C min^{-1} under nitrogen atmosphere (40 mL min^{-1}). The instrument used for the dynamic mechanical analysis (DMA) was a Q800 V20.24 Build 43. Before the analysis, the samples were placed in a climatic chamber with 50% humidity and a temperature of 23 °C. A strain of 0.2% and a preload of 0.01 N were applied and the ramp temperature was 2 °C min^{-1}. For testing, the membrane was cut in 30 mm x 0.6 mm strips with a thickness of ≈150 µm.

2.5. Cell Assembly and Electrochemical Testing

The soaking properties of the three separators were evaluated by calculating the uptake (η) percentage by measuring the weight of each membrane before soaking (W_0) and after 6 h of immersion in the electrolyte (W_1) (Equation 1). The membrane mass was measured using a precision balance subsequent to the elimination of surplus surface solution via filter papers. For all measurements, LP30 was used as the electrolyte. For each sample, the measurement of electrolyte uptake was conducted a minimum of three times, and the average values were subsequently calculated.

$$\eta = \frac{W_1 - W_0}{W_0} * 100\ \% \tag{1}$$

For ionic conductivity measurements, the membranes were sandwiched between two stainless steel blocking electrodes after a 12 h immersion in the electrolyte. The measurements were conducted in electrochemical battery test cells with reference electrodes (model ECC-Ref, EL-cell, Germany) using an alternating voltage signal of 10 mV within the frequency range of 200 kHz to 100 mHz, with a membrane diameter of 18 mm. All Nyquist plots obtained through EIS were analyzed using the non-linear least squares (NLLS) method (RQ equivalent circuit). The ionic conductivity (σ) was calculated from Equation (2).

$$\sigma = \frac{l}{A \cdot R}\left[S\ cm^{-1}\right] \tag{2}$$

where l and A represent the thickness and effective area of the membrane, respectively, and R denotes the resistance determined from the Nyquist plot in the conducted test.

The electrochemical stability window (ESW) of the separators was evaluated through cyclic voltammetry (CV) and linear sweep voltammetry (LSV). In both cases, a Li-metal vs. carbon-coated copper (for CV) or vs. carbon-coated aluminum (for LSV) cell configuration was employed, with a scan rate of 0.1 mV s^{-1}.

For the evaluation of plating and stripping reversible cycling, symmetric lithium-metal cells were assembled using PVB-based membranes soaked with 200 µL of LP30 electrolyte. The plating and stripping measurements involved galvanostatic cycling at ambient temperature employing a current density of 0.05 mA cm^{-2} for 3 h in both charge and discharge steps. Throughout the cycling, EIS was performed every 5 cycles at the open circuit voltage (OCV) with an oscillating potential of 10 mV in the 300 kHz – 0.1 Hz frequency range.

The electrochemical performance in Li-metal cells was evaluated on a laboratory scale with ECC-Ref EL-cells. The setup included lithium metal as the anode, $LiFePO_4$ (LFP) as the cathode, the prepared PVB membrane as the separator, and LP30 as the electrolyte. For the cathode preparation, a solution of poly(acrylic acid) (PAA) in ethanol (from Sigma-Aldrich) was prepared and stirred. The mixture of active materials and conductive carbon Super C65 (Timcal) was obtained by mixing and grinding. This mixture was then added to the solution, resulting in a slurry with an active material:Super C65:PAA composition of 80:10:10 (mass ratio). The stirring process continued for 6 h until a homogeneous slurry was obtained. Subsequently, the slurries were doctor-bladed onto aluminum foil with a 150 µm gap. The layers were heated at 70 °C for 2 h and then dried at room temperature. Finally, the layers were pressed and cut. The galvanostatic charge-discharge measurements were conducted using an ARBIN BT2000 battery tester within a voltage range of 2.5 to 3.8 V vs. Li^+/Li at a current rate of C/10, with 1 C assumed to be 170 mA g^{-1} (with respect to the active material mass). During the initial cycles, lower current rates (C/20) were used to ensure the proper stabilization of the electrode-electrolyte interphase. Every test cell was assembled inside an Ar-filled glove box to avoid moisture contamination and left for 6 h at OCV before running the measurements.

3. Results and Discussion

3.1. Materials Characterization

Commercial PVB, the H_{12}MDI isocyanate, porous and dense membranes were analyzed by means of IR spectroscopy (**Figure 2a**). The IR spectrum of commercial PVB displays many absorption bands in the whole IR region, characteristic of its different functional groups: particularly, the spectrum shows a broad band

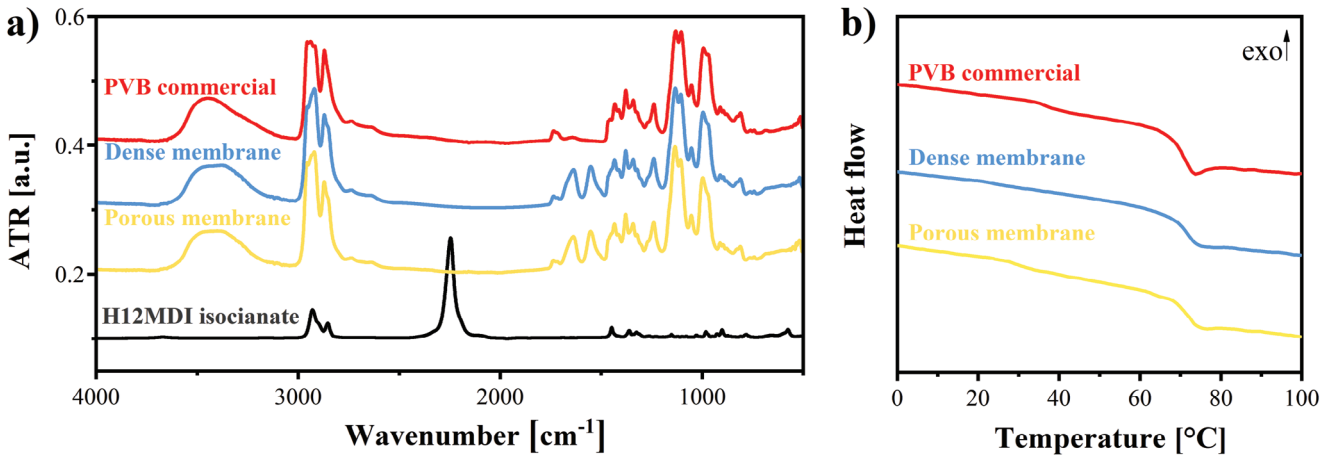

Figure 2. a) IR spectra were collected in ATR mode of commercial PVB, H_{12}MDI isocyanate, and the two membranes. The intensities of spectra of PVB-containing materials have been normalized with respect to the fingerprints below 1500 cm^{-1}, while the intensity of the spectrum of H_{12}MDI isocyanate has been normalized based on its contribution to the $\nu(CH_x)$ absorption in the spectra of the membranes. b) DSC thermograms during the second heating cycle of pristine commercial PVB, porous and dense membranes obtained after the cross-linking process.

centered at 3440 cm^{-1}, which is assigned to the stretching of the —OH groups (quantified as 0.0172 mol g^{-1} of PVB) in interaction within the polymer chains and with physisorbed water, a complex envelope of bands between 3000 and 2800 cm^{-1} due to $\nu(CH_x)$, a well-defined band at 1735 cm^{-1} assigned to ν(C═O) of a carbonyl ester,[45] indicative of the presence of the acetate pendants, and the molecular fingerprints below 1500 cm^{-1}, including ν(C—O), ν(C—C), and all the bending modes of the chains. Unfortunately, the dioxane moieties have no specific bands that can univocally identify their presence. In general, as shown in Figure S4 (Supporting Information), the spectrum of commercial PVB can be well reproduced by a combination of the spectra of a linear alkane, ethyl acetate, a secondary alcohol, and 1,3-dioxane.

On the other side, the spectrum of H_{12}MDI is dominated by the characteristic absorption band of asymmetric ν(N═C═O) at 2248 cm^{-1}, coupled with the much weaker band of symmetric ν(N═C═O) at 1450 cm^{-1}.[46] That signal is completely absent in the spectra of the two membranes, confirming that all the H_{12}MDI isocyanate has been involved in the crosslinking of PVB chains.

The spectra of the two membranes are mostly overlapped with each other and almost coincide with the spectrum of commercial PVB, except for two intense bands at 1638 and 1552 cm^{-1}. Those bands are characteristic of the urethane bond,[47] the former due to ν(C═O) vibrational mode (particularly, shifted at lower wavenumbers because the bond strength is weakened by possible resonance with the resonant structure O^-—C═N^+),[48] the latter deriving from the overlap of δ(N—H) and ν(C—N) absorption bands[49] (in some cases those two bands are even observed separated from each other,[50] when the contribution of O^-—C═N^+ resonance is minor and ν(C—N) is normally positioned below 1400 cm^{-1}).

Thermogravimetric analysis (TGA) analysis was carried out to compare the thermal stability of the commercial and crosslinked PVB-based membranes, to evaluate their possible use as separators in LIBs. In Figure S5 (Supporting Information), a comparison between the thermograms of the pristine commercial PVB and the two crosslinked dense and porous polymers obtained from the coagulation bath is shown. Commercial PVB shows a $T_{5\%}$ at 325 °C, while the crosslinked porous PVB starts degrading at 295 °C and the dense sample at 284 °C (**Table 1**). In this case, the crosslinking affects the thermal stability of the crosslinked polymers, which probably start degrading directly from the linker. Evaluating the $T_{50\%}$ instead, a reverse trend can be observed, even if in a reduced way. This probably confirms that the PVB cannot be thermally stabilized by this type or degree of crosslinking, and the first fragment generated during the decomposition is the crosslinker itself, as also suggested by the weight loss ≈20 wt.% for both crosslinked samples, which is the quantity introduced during the crosslinking procedure.

Nevertheless, all resulting crosslinked membranes were stable up to ≈280 °C, which is more than sufficient for standard temperature operation in LIBs. In this work, all the electrochemical results were carried out at ambient laboratory temperature (≈25 °C).

Differential scanning calorimetry (DSC) measures were carried out to evaluate possible changes in the glass transition temperatures of PVB after the crosslinking process (Figure 2b). As reported in the complete thermograms in Figure S6a (Supporting Information), the commercial PVB shows some chain relaxation and molecular rearrangements during the first heating cycle resulting in a broad endothermic peak, which then disappeared during the second cycle, while the T_g is clearly visible even in the second heating cycle in Figure 2b at 70.6 °C, in agreement with the reported literature.[51] Both the T_g values of the dense and the porous membranes are not affected by the crosslinking, showing

Table 1. Thermal stability of the commercial and crosslinked PVB at 5% ($T_{5\%}$) or at 50% ($T_{50\%}$) weight loss.

Sample	$T_{5\%}$ [°C]	$T_{50\%}$ [°C]
Commercial PVB	325	375
Porous PVB membrane	295	380
Dense PVB membrane	284	387

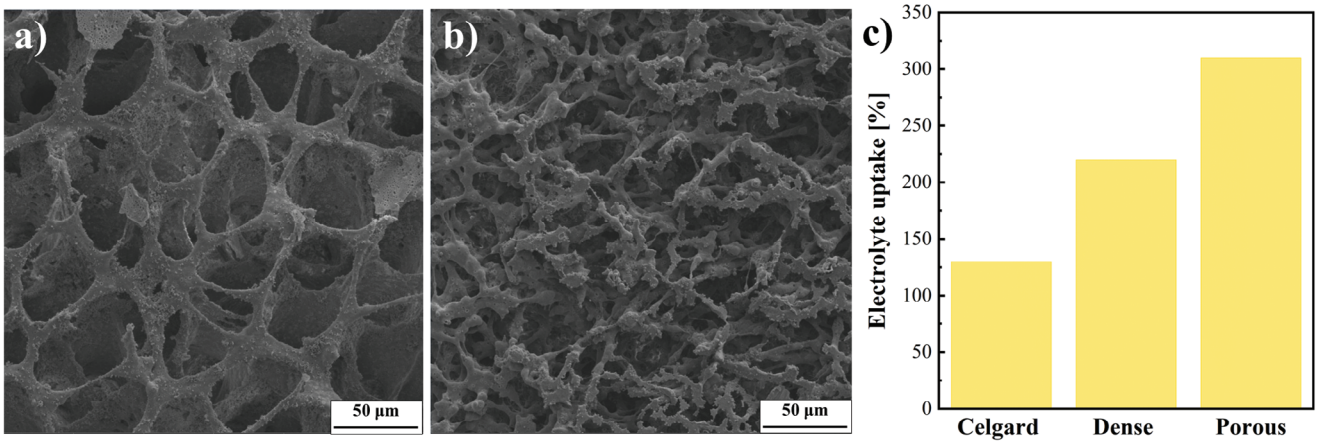

Figure 3. FESEM images of the PVB-based mambranes: a) porous and b) dense membrane; c) soaking test for Celgard®2400, porous and dense membranes, obtained by soaking them for 6 h in the LP30 electrolyte.

a T_g of 70.9 and 71.0 °C, respectively. This demonstrates the low degree of crosslinking, linked to the low quantity of isocyanate introduced during the reaction, able to react with a limited amount of —OH groups potentially available for the crosslinking.

Dynamic mechanical analysis (DMA) was carried out to evaluate the mechanical properties of the crosslinked porous and dense PVB-based polymer membranes. After two repeated measures per sample, the storage modulus at room temperature resulted in 220 MPa (value averaged between the two values obtained from DMA) for the dense membrane and 65 MPa for the porous one (Figure S6b, Supporting Information). Besides, the DMA thermograms shown in Figure S6b (Supporting Information) pointed out a T_α at 74 °C, in good agreement with the T_g previously evaluated by DSC analysis. Even if the modulus is not sufficiently high to avoid the lithium dendrites, it can assure good handleability of the resulting membranes and good adhesion to the lithium and the cathode.

3.1.1. Membrane Morphology and Soaking Properties

The surface morphology of the membranes was investigated using FESEM (**Figure** 3a,b). The average pore size in the porous and dense membranes resulted 55 and 10 µm, respectively. The porous separator, characterized by relatively larger pores, is susceptible to penetration by Li dendrites,[52] which may pose risks to both the safety and cycle stability of batteries. It is well-established that a separator distinguished by adequate porosity and electrolyte absorption properties can augment the efficiency of battery assembly and facilitate the movement of lithium ions between electrodes. Therefore, the soaking test is imperative for quantifying the weight alteration of the membrane subsequent to electrolyte soaking, thus evaluating the uptake capacity of the material network.[53]

As shown in Figure 3c, Celgard®2400 monolayer PP separator, dense and porous membranes showed a percentage uptake of 130, 220, and 310%, respectively. Thus, porous and dense membranes exhibit higher uptake compared to Celgard®2400. Specifically, the porous membrane possesses the highest porosity and the lowest weight, consequently resulting in a notably elevated electrolyte uptake.

3.2. Ionic Conductivity and Electrochemical Behavior of PVB-Based Polymer Membranes

Ionic conductivity serves as a crucial metric in assessing the suitability of a separator for LIBs, exerting a substantial influence on battery performance.[15] **Figure** 4 shows the EIS data of Celgard®2400 separator, porous and dense membranes, after soaking for 12h in the liquid electrolyte (i.e., involving only the uptaken electrolyte as shown in Figure 3c). The ionic conductivity of both membranes under study (dense and porous) is nearly equivalent to that of the Celgard®2400 monolayer PP membrane used as a benchmark (and of other commercial

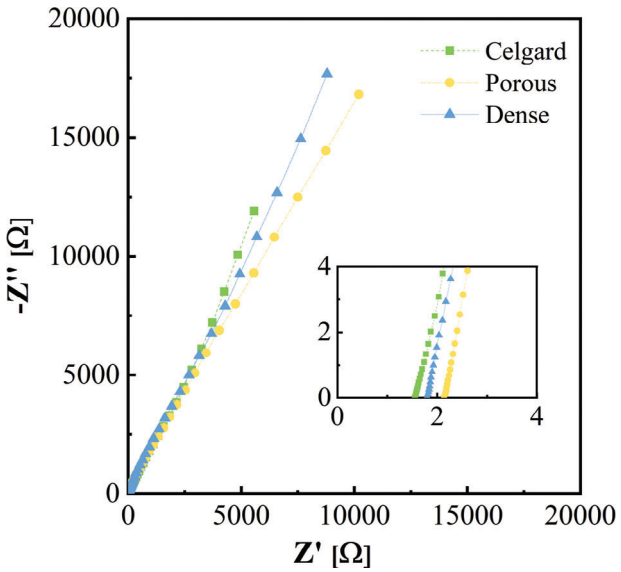

Figure 4. EIS results (Nyquist plot) of Celgard®2400, porous and dense membranes after soaking for 12 h in LP30 electrolyte.

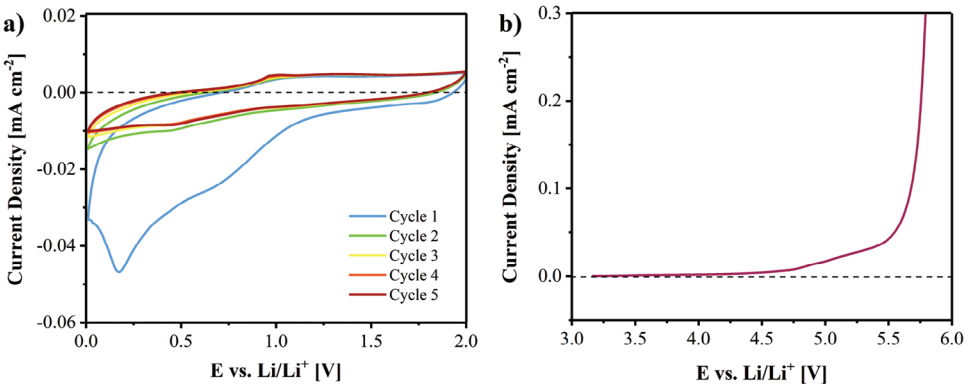

Figure 5. Electrochemical stability window (ESW) of the dense PVB-based mambrane: a) CV and b) LSV.

separators reported in the literature[54]), with values in the range of 0.25–0.35 mS cm^{-1}. The ionic conductivity of the PVB-based membrane is mainly related to the porous structure that forms an extended channel net, thus enabling high electrolyte uptake and remarkable lithium-ion mobility.[55]

The ESW represents an essential parameter when evaluating the performance of an electrolyte material, as it assesses its inherent stability and the interfacial compatibility between the separator and the electrodes.[56] ESW of the dense membrane was investigated at the cathodic side through a CV test and at the anodic side through an LSV test (**Figure 5**). Starting from the cathodic stability (Figure 5a), the membrane resulted to be stable in the whole measurement range (0–2 V vs Li$^+$/Li); CV profiles are reversible and phenomena related to the SEI formation on the carbon-coated copper are notable within the range of 0.7–0.15 V versus Li$^+$/Li during the first cycle.[57] The formation of SEI is a crucial and irreversible process as it hinders additional parasitic reactions, allowing proper cell cycling.[58–60] In successive cycles, the SEI stabilizes and acts as a protective layer. Nonetheless, two small peaks at 0.5 V during reduction and 1.0 V during oxidation appear, which can be correlated with the reversible intercalation of lithium in the carbon-based material.[61] On the anodic side, during the LSV (Figure 5b) the membrane showed to be stable up to 4.7 V vs. Li$^+$/Li, indicating good electrochemical and interfacial compatibility.[62]

Galvanostatic cycling was conducted at a current density of 0.05 mA cm^{-2} with a cycle duration of 6 h in a symmetrical Li cell using both porous and dense membranes to investigate the Li plating and stripping processes, and in order to shed light on the kinetics of the cycling process and their reversibility. EIS was measured for both membranes before cycling at the open circuit voltage (OCV) and every 5 cycles during stripping deposition (Figure S7, Supporting Information). By using the porous membrane, the overall resistance at OCV was ≈770 Ω, but then it decreased to ca. 44 Ω upon cycling (with also the recorded overpotential decreasing consequently); such a reduction in resistance may be related to the activation reaction on the surface during early-stage cycles.[63] However, after 90 h of galvanostatic cycling, a short-circuit occurred, presumably due to the larger pores in the porous membrane, which are susceptible to penetration by Li dendrites.[52,64] In contrast, the symmetric cell with the dense membrane showed a very low initial resistance (ca. 30 Ω at OCV), which increased slightly before stabilizing at ca. 60 Ω for more than 40 cycles. The dense membrane displayed smooth Li stripping and deposition profiles upon cycling, with negligible polarisation by the end of the testing period.[65,66]

3.3. Recycled PVB-Based Membranes

As a final proof of concept, membranes were prepared also with PVB recycled from the waste of automotive glasses, obtained by the partners in the H2020 *SUNRISE* consortium. This specific recycled PVB (re-PVB) was studied in a previous work using FT-IR, TGA, and NMR. From those analyses, re-PVB resulted in containing different compounds as plasticizers, all belonging to the diester class, with a weight ratio between polymer and plasticizers roughly close to 1:1.[44] This led to an impure and highly sticky slurry, needing, therefore, the ratio between polymer and crosslinker to be adapted, passing from 5:1 to 20:1. Water was chosen as a unique coagulation bath medium, since no difference in the morphology was observed when using NMP-water mixture. The resulting membrane presented a dense and packed morphology (see FESEM images shown in **Figure 6**a,b). The microstructure visibly differs from the previous membranes obtained by using pure, commercial PVB. The difference is caused by the sizeable amount of plasticizers in the PVB flakes,[40] which clearly persist also after the preparation. From a macroscopic point of view (Figure 6c), a difference between the commercial PVB-derived and the re-PVB membrane is also evident: the latter appears more translucent, indicating a lower level of crystallinity compared to the former membrane.[67] Also in this case, the formation of urethane bonds was assessed by IR spectroscopy (Figure S8, Supporting Information): the spectra of re-PVB flakes and re-PVB-based membrane display the same absorption bands of commercial PVB and PVB-based membranes (the two bands of urethane bonds at 1638 and 1552 cm^{-1} respectively, much less intense because of the lower degree of crosslinking with respect to the membranes obtained from commercial PVB). Additional signals are present due to the presence of plasticizers, typically containing ester groups (whose stretching mode gives rise to an intense band at 1730 cm^{-1}).[44]

Regarding thermal stability, the degradations of both pristine re-PVB flakes and crosslinked re-PVB start at lower temperatures, and the different degradation steps are mainly related to the plasticizers used in the formulation (Figure S9, Supporting

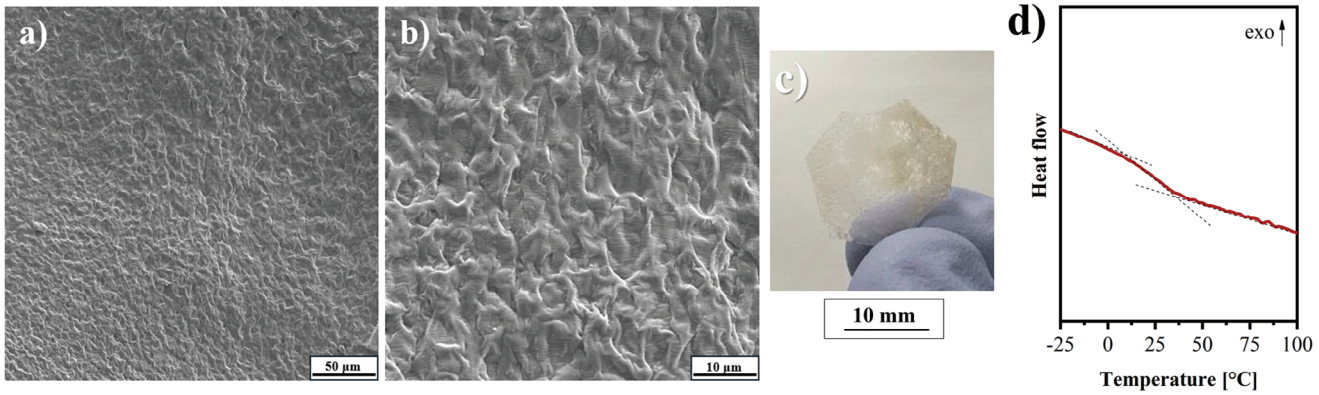

Figure 6. FESEM images of the membrane prepared with pure H_2O-based coagulation bath with two different zooms: a) 50 µm and b) 10 µm. c) Digital photograph of the re-PVB membrane. d) DSC analysis of re-PVB-based membrane.

Information). In **Table 2**, the $T_{5\%}$ and $T_{50\%}$ are listed. Also in this case, the crosslinking slightly affects the thermal stabilities, because the crosslinking units represent a favorable breaking point hence lowering the onset temperature of the degradation ($T_{5\%}$) of ≈20 °C.

The DSC thermogram of the re-PVB membrane (Figure 6d) showed a broad signal related to the glass transition, starting well below the room temperature (at ≈10 °C) and spreading for more than 25 °C because of the presence of plasticizers and contaminants.

Considering the DMA analysis (Figure S10, Supporting Information), results show a storage modulus for pristine re-PVB that is ≈60 MPa at room temperature, similar to what is reported for cross-linked re-PVB: the cross-linking should not increase the final value, that is sufficient enough to enable the use of the resulting membrane as a separator for lithium cells, able to cycle at room temperature. Also, in this case, the T_g is very broad at ≈35 °C.

Galvanostatic plating/stripping measurements were conducted also for the recycled PVB-based membrane to investigate its stability and compatibility at the interface with the lithium metal anode[65] (**Figure 7a**). EIS was performed before cycling at the open circuit voltage (OCV) and during stripping deposition to check the cell status and the variation of resistance (Nyquist plots in Figure 7b, while resistance values in Figure 7c). The EIS data have been fitted with RelaxIS software (rhd instruments, Germany) by using the equivalent circuit sketched in Figure 7d, where: i) $R_{LE,bulk}$ represents bulk resistance of liquid electrolyte; ii) $R_{SEI,bulk}$ and C_1 are assigned to the semicircle at high frequencies and correspond to bulk resistance and capacitance of the SEI layer, partly overlapped by iii) $R_{Li/SEI}$ and C_2, which are related to semicircle at middle frequencies and describe interfacial charge transfer from the SEI to the metal Li and capacitance; iv) $R_{LE/SEI}$ and C_3 are related to the semicircle at low frequencies and correspond to the charge transfer from the liquid electrolyte to the SEI resistance and the capacitance.[63] The plating and stripping measurement shows a high initial overpotential of ≈0.8 V. The high value is related to a high initial ohmic and charge transfer resistances. The overpotential gradually decreases upon cycling, reaching a stable value of ≈± 0.2 V after 200 h. The diminution is related to interface stabilization. Indeed, the SEI layer is considered to be formed by two parts: a thin (nm) and porous-less SEI layer, which is in contact with lithium metal, and a porous, thicker SEI layer (µm) at the electrolyte side. The transport across the thin compact sublayer primarily consists of the migration of Li^+ ions. Conversely, the transport across the porous, thicker part of SEI also involves the anions in the electrolyte to the pores.[68,69]

The trend may be related to an initial activation and stabilization process, which terminates later with improved interface compatibility, thus represented by the diminished overpotential value. The improved compatibility cannot be ascribed to membrane-related phenomena only; indeed, it is likely associated also with the increased porosity of lithium metal, which is acquired by prolonged plating and stripping processes. Thanks to an increased porosity, an increased surface is also reached, which leads to easier lithium stripping and deposition.[68] Indeed, the remaining cycling appears to be stable at ±0.2 V over 600 h. This value is also coherent with the previous plating and stripping measurement conducted on commercial PVB-derived membranes (Figure S7, Supporting Information), in which the stabilization is also reached after approximately the same number of hours. Overall, during cycling, small plateaux are visible, which are signs of a not completely homogenous lithium deposition over the lithium metal surface,[70] which therefore appears to happen at different potential values.

Deepening EIS analyses (Figure 7b,c), in addition to an initial resistance value of 12 Ω, associated with the bulk resistance of liquid electrolyte ($R_{LE,bulk}$) and a small arc with the value of 4 Ω at higher frequency related to bulk resistance of the SEI layer ($R_{SEI,bulk}$), a second major, wider arc at medium-low frequencies is observable, which is likely associated with charge transfer resistance ($R_{Li/SEI}$ and $R_{LE/SEI}$). The latter is likely related to ion diffusion resistance in the proximity of the anode metal

Table 2. Thermal stability of the pristine re-PVB flakes and re-PVB membrane at 5% ($T_{5\%}$) or at 50% ($T_{50\%}$) weight loss.

Sample	$T_{5\%}$ [°C]	$T_{50\%}$ [°C]
re-PVB	244	360
re-PVB membrane	228	369

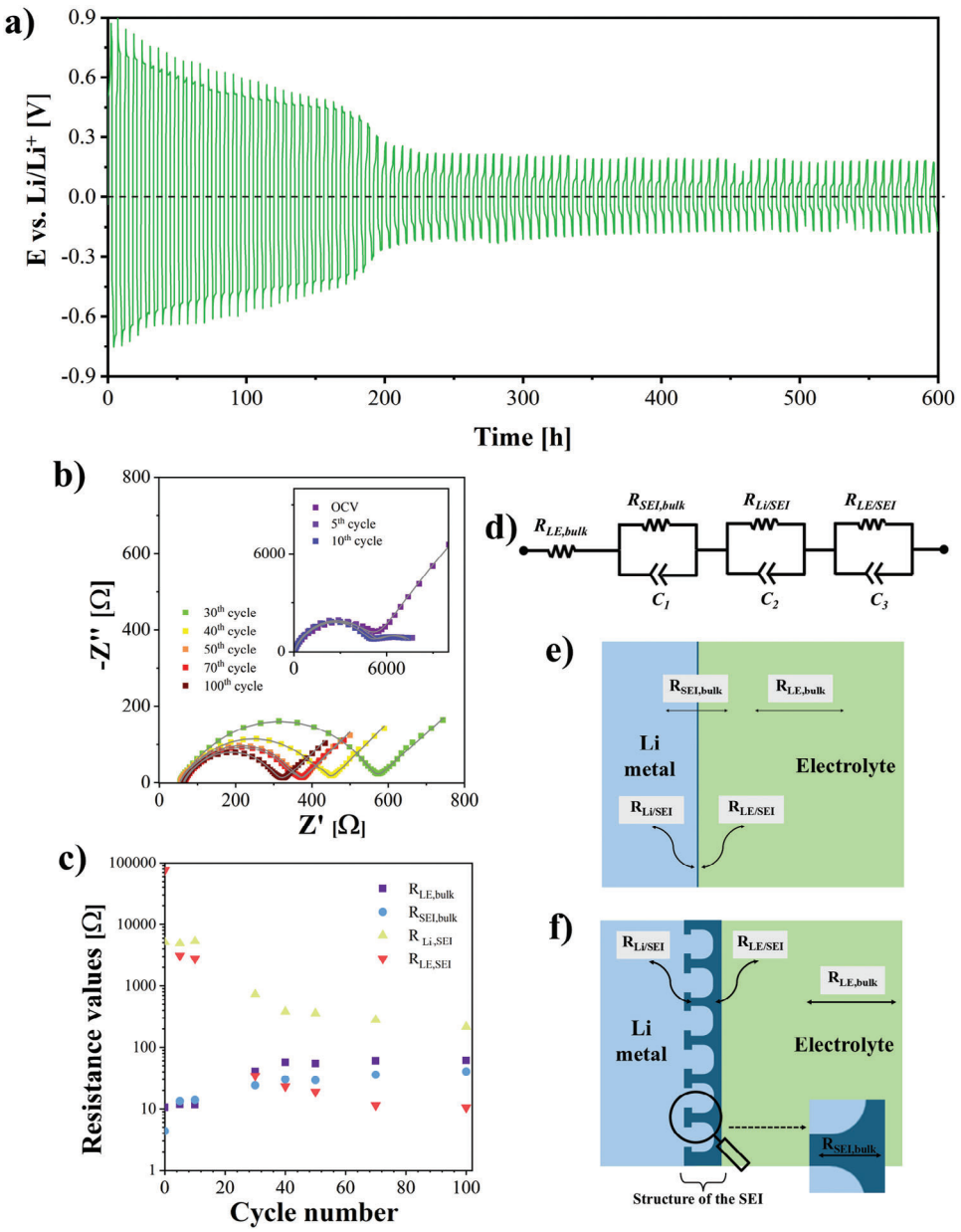

Figure 7. a) Plating and stripping measurements over 600 cycles of the re-PVB-based membrane in a symmetrical Li-metal cell with LP30 as electrolyte. b,c) Electrochemical impedance spectroscopy of the re-PVB membrane, acquired every 10 cycles of plating and stripping. d) Corresponding equivalent circuit of the system, where $R_{LE,bulk}$ is the bulk resistance of liquid electrolyte, $R_{SEI,bulk}$ is the bulk resistance of the SEI layer, $R_{LE/SEI}$ and $R_{Li/SEI}$ are the charge transfer resistances from liquid electrolyte to SEI bulk and from SEI bulk to the anode structure. Schematic representations of the resistance contributions in a Li|Li symmetrical cell e) before and f) after cycling, where dendritic formation is also visible.

surface.[63] These results are in line with the high initial overpotential registered during plating/deposition measurements (Figure 7a). Indeed, during this analysis, the resistance values related to the charge transfer decrease drastically, as also the overpotential decreases plentifully after circa 200 h. As in the previous case of the porous membrane (Figure S7a,b, Supporting Information), the overall resistance decrease may be related both to the activation reactions at the surface during early-stage cycles,[63] as well as to an enlarged surface area of the lithium metal anode after repeated plating. Contrarily to the porous membrane, in which the enlarged area is likely consequent to dendritic formation that leads to short circuit after 90 h of plating and stripping,[64] in the re-PVB-based membrane case, the separator function is preserved along cycling, showing an improved interface compatibility, thus avoiding short circuit phenomena and achieving 600 h of measurement. Overall, charge transfer phenomena across the SEI to/from the porous structure of the metal Li ($R_{Li,SEI}$) mainly contribute to the overall system resistance. Therefore, the re-PVB-based membrane allows the ionic transfer without being damaged by dendritic growth; thus,

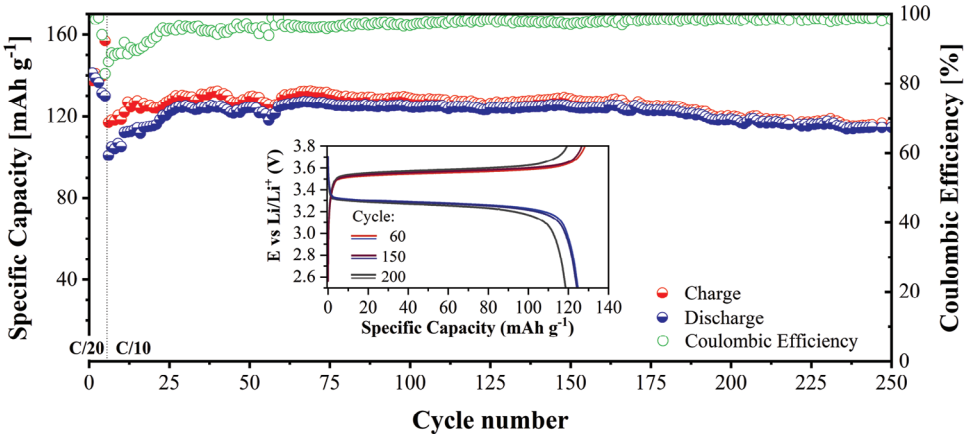

Figure 8. Specific capacity and coulombic efficiency of the re-PVB-based membrane soaked in LP30 electrolyte in Li ‖ LFP cell configuration, recorded in the 2.5–3.8 V versus Li^+/Li range at ambient laboratory temperature.

it properly operates as a self-standing and mechanically robust separator over very prolonged cycling.

The ESW of the re-PVB-based membrane is reduced in comparison to the membrane prepared with commercial PVB (Figure S11, Supporting Information), due to the presence of plasticizers and additives, with degradation starting at 4.2 V versus Li^+/Li. Nevertheless, this window is still compatible with commercial cathodes, like $LiFePO_4$ (LFP). Indeed, as proof of concept, for the first time, the recycled-PVB-based membrane was soaked in standard LP30 liquid electrolyte and tested in a lab-scale Li-metal cell with LFP as the cathode (**Figure 8**). The cell was first cycled at C/20 over 5 cycles to achieve a stable SEI formation. In this phase, the SEI formation takes place and low currents facilitate side reactions,[71] thus affecting specific capacity and efficiency values. Nevertheless, the current rate was successively increased to C/10 and maintained for the rest of the long-term cycling test. The increase in current density is correlated to a slight decrease in specific capacity values due to ohmic polarization effect.[72] Overall, after an initial activation period where specific capacity and efficiency values slightly fluctuated at ≈120 mAh g^{-1}, cell behavior tended to stabilize after 60 cycles, achieving a stable capacity exceeding 120 mAh g^{-1} at C/10 up to 250 cycles, with excellent Coulombic efficiency approaching 100%. Some significant voltage profiles of LFP are shown in the inset of Figure 8, characterized by a flat plateau and well-overlapped with each other, thus demonstrating the good stability of the whole electrochemical system over time upon the charge/discharge processes.

These results are coherent with the plating and stripping outcomes obtained both for the commercial PVB-based and the re-PVB-based membranes. The Li-metal cell shows stable prolonged cycling at ambient temperature, which accounts for the high (electro)chemical stability of the recycled-PVB-based polymer separator developed in this work and its potential use in LIB with standard commercial electrode/electrolyte components.

4. Conclusion

In this work, we successfully prepared by phase inversion technique (coagulation bath) a polymeric membrane by reacting PVB with H_{12}MDI as a crosslinking agent. Depending on the type of coagulation bath, both porous and dense membranes were obtained. Both membranes were characterized from a physicochemical point of view and then used as separators in lab-scale lithium-based electrochemical cells. The PVB-based membranes exhibited adequate thermal and mechanical stability (degradation temperature above 300 °C and storage modulus up to 220 MPa), good durability, and interfacial compatibility with Li metal upon plating and stripping for almost 800 h. As proof of concept, within the framework of the H2020 European *SUNRISE* project, the same membranes were prepared using recycled PVB (re-PVB), obtained from recovered wastes of automotive glasses. The re-PVB-based membrane was evaluated through a Li plating/stripping test, showing long durability and compatibility with metal lithium. Successively, the membrane was used as a separator in a Li-metal cell with a LFP cathode, achieving a stable capacity of 120 mAh g^{-1} at C/10 along 250 cycles (≈80% of LFP practical capacity), and showing cycle stability up to 250 cycles (with a Coulombic efficiency increasing over time and approaching 100%). These results, for the first time, highlight the practical potential and feasibility of using recycled PVB membranes as separator in LIBs, allowing greener and more sustainable battery production in a circular economy perspective.

Supporting Information

Supporting Information is available from the Wiley Online Library or from the author.

Acknowledgements

The SUNRISE project (https://sunrise-project.eu/) has received funding from the European Union's Horizon 2020 Research and Innovation Program under grant agreement No 958243. A.P. gratefully acknowledges the Italian Ministry for University and Research (MUR) for funding under the D.M. 1062/2021 program.

Open access publishing facilitated by Politecnico di Torino, as part of the Wiley - CRUI-CARE agreement.

Conflict of Interest

The authors declare no conflict of interest.

Data Availability Statement

The data that support the findings of this study are available from the corresponding author upon reasonable request.

Keywords

lithium battery, polyurethane, polyvinyl butyral, recycling, separator

Received: August 1, 2024
Revised: September 13, 2024
Published online:

[1] M. Hafner, S. Tagliapietra, *The Global Energy Transition: A Review of the Existing Literature*, (Eds.: M. Hafner, S. Tagliapietra), *in*: The Geopolitics of the Global Energy Transition, Springer International Publishing, Cham, **2020**, pp. 1–24.
[2] K. Shivarama Krishna, K. Sathish Kumar, *Renewable and Sustainable Energy Reviews* **2015**, *52*, 907.
[3] A. Kalair, N. Abas, M. S. Saleem, A. R. Kalair, N. Khan, *Energy Storage* **2021**, *3*, e135.
[4] Y. Yang, S. Bremner, C. Menictas, M. Kay, *Renewable Sustainable Energy Rev.* **2018**, *91*, 109.
[5] M. Yoshio, R. J. Brodd, A. Kozawa, *Lithium-Ion Batteries*, 1st ed., Springer, New York **2009**.
[6] B. Scrosati, J. Garche, *J. Power Sources* **2010**, *195*, 2419.
[7] C. Daniel, J. O. Besenhard, *Handbook of battery materials*, 2nd ed., John Wiley & Sons, Weinheim, **2012**.
[8] C. Zenghua, W. Jiantao, W. Zhaohui, Z. Jinling, L. Shigang, *Progress in Chemistry* **2018**, *30*, 1960.
[9] A. Ponrouch, D. Monti, A. Boschin, B. Steen, P. Johansson, M. R. Palacín, *J. Mater. Chem. A* **2015**, *3*, 22.
[10] L. Li, H. Cheng, J. Zhang, Y. Guo, C. Sun, M. Zhou, Q. Li, Z. Ma, J. Ming, *ACS Energy Lett.* **2023**, *8*, 1076.
[11] N. Badi, A. M. Theodore, S. A. Alghamdi, H. A. Al-Aoh, A. Lakhouit, P. K. Singh, M. N. F. Norrrahim, G. Nath, *Polymers* **2022**, *14*, 3101.
[12] J. Zheng, W. Li, X. Liu, J. Zhang, X. Feng, W. Chen, *Energy Environ. Mater.* **2023**, *6*, e12422.
[13] J. Liang, J. Luo, Q. Sun, X. Yang, R. Li, X. Sun, *Energy Storage Mater.* **2019**, *21*, 308.
[14] J. Zhang, X. Yao, R. K. Misra, Q. Cai, Y. Zhao, *J. Mater. Sci. Technol.* **2020**, *44*, 237.
[15] P. Arora, Z. Zhang, B. Separators, *Chem. Rev.* **2004**, *104*, 4419.
[16] J. Choi, P. J. Kim, *Current Opinion in Electrochemistry* **2022**, *31*, 100858.
[17] C. Vaalma, D. Buchholz, M. Weil, S. Passerini, *Nat. Rev. Mater.* **2018**, *3*, 18013.
[18] C. Carrot, A. Bendaoud, C. Pillon, *Handbook of Thermoplastics*, 2nd ed. CRC Press, London , **2015**, pp. 89–137.
[19] M. Martín, X. Centelles, A. Solé, C. Barreneche, A. I. Fernández, L. F. Cabeza, *Constr. Build. Mater.* **2020**, *230*, 116897.
[20] X. Zhang, H. Hao, G. Ma, *Engineering Structures* **2013**, *56*, 1707.
[21] M. Ude, M. Ashraf-Khorassani, L. Taylor, *Chromatographia* **2002**, *55*, 743.
[22] A. Mańin, L. Tatarenko, Y. A. Shlyapnikov, *Solubility of antioxidants in poly (vinyl butyral)* **1998**, *62*, 507.
[23] S. Khouri, M. Behun, L. Knapcikova, A. Behunova, M. Sofranko, A. Rosova, *Energies* **2020**, *13*, 5391.
[24] X. Huang, Y. Lin, G. Fang, *Sol. Energy* **2018**, *161*, 187.
[25] C. Carrot, A. Bendaoud, C. Pillon, O. Olabisi, K. Adewale, *Polyvinyl butyral, Handbook of thermoplastics* **2016**, *2*, 89.
[26] MarketsandMarkets, Polyvinyl Butyral (PVB) Market by Applications and Region - Global Forecast to 2027, **2024**.
[27] M. Królikowski, P. Żach, M. Kalestyński, *Polymers* **2022**, *14*, 5119.
[28] B. Swain, J. R. Park, C. G. Lee, *J. Cleaner Prod.* **2022**, *334*, 130192.
[29] B. Guner, Y. E. Bulbul, N. Dilsiz, *J. Taiwan Inst. Chem. Eng.* **2022**, *132*, 104136.
[30] M. Hestin, S. de Veron, S. Burgos, *Deloitte Sustainability* **2016**.
[31] T. Yokozawa, A. Yokoyama, *Chem. Rev.* **2009**, *109*, 5595.
[32] K. Ashida, *Polyurethane and Related Foams*, 1st ed. CRC Press, Boca Raton, **2006**.
[33] M. Szycher, *Polyurethanes, Szycher'S Handbook of Polyurethanes*, CRC Press Taylor & Francis Group, Boca Raton, FL, USA, **2013**, pp. 1–12.
[34] M. S. M. Misenan, A. S. A. Khiar, T. Eren, *Polym. Int.* **2022**, *71*, 751.
[35] Z. Lv, Y. Tang, S. Dong, Q. Zhou, G. Cui, *Chem. Eng. J.* **2022**, *430*, 132659.
[36] Y. Liu, R. Tao, S. Chen, K. Wu, Z. Zhong, J. Tu, P. Guo, H. Liu, S. Tang, J. Liang, Y.-C. Cao, *J. Power Sources* **2020**, *477*, 228694.
[37] L. Wu, F. Pei, D. Cheng, Y. Zhang, H. Cheng, K. Huang, L. Yuan, Z. Li, H. Xu, Y. Huang, *Adv. Funct. Mater.* **2024**, *34*, 2310084.
[38] R. Andersson, G. Hernández, J. See, T. D. Flaim, D. Brandell, J. Mindemark, *ACS Appl. Energy Mater.* **2022**, *5*, 407.
[39] F. Lian, Y. Wen, Y. Ren, H. Guan, *J. Membr. Sci.* **2014**, *456*, 42.
[40] Z. Xu, W. Li, Z. Chen, D. Wang, T. Feng, H. Potapenko, M. Wu, *Macromol. Mater. Eng.* **2019**, *304*, 1800477.
[41] C. Fernández Acevedo, L. Martínez De Morentín Osaba, E. Osés Arteta, G. Medina Herrera, M. A. Fernández Fernández, Polyvinyl Butyral Recycling Method. Patent EP2308919A1 **2011**.
[42] G. M. M. Sadeghi, J. Morshedian, M. Barikani, *Polym. Test.* **2003**, *22*, 165.
[43] B. Díez, R. Rosal, *Nanotechnology for Environmental Engineering* **2020**, *5*, 15.
[44] V. Nikitakos, A. D. Porfyris, K. Beltsios, C. Papaspyrides, S. Bordignon, M. R. Chierotti, S. Nejrotti, M. Bonomo, C. Barolo, A. Piovano, *Polymers* **2023**, *16*, 10.
[45] S. C. Edington, J. C. Flanagan, C. R. Baiz, *The Journal of Physical Chemistry A* **2016**, *120*, 3888.
[46] R. P. Hirschmann, R. N. Kniseley, V. A. Fassel, *Spectrochimica Acta* **1965**, *21*, 2125.
[47] Y. Ji, X. Yang, Z. Ji, L. Zhu, N. Ma, D. Chen, X. Jia, J. Tang, Y. Cao, *ACS Omega* **2020**, *5*, 8572.
[48] K. Nakayama, T. Ino, I. Matsubara, *J. Macromolecular Sci.—Chem.* **1969**, *3*, 1005.
[49] C. Zhang, Z. Ren, Z. Yin, H. Qian, D. Ma, *Polym. Bull.* **2008**, *60*, 97.
[50] M. Bonomo, B. Taheri, L. Bonandini, S. Castro-Hermosa, T. M. Brown, M. Zanetti, A. Menozzi, C. Barolo, F. Brunetti, *ACS Appl. Mater. Interfaces* **2020**, *12*, 54862.
[51] J. D. Ambrosio, M. Sonego, L. H. Staffa, M. A. Chinelatto, L. C. Costa, *Composites, Part B* **2019**, *175*, 107118.
[52] A. Jana, D. R. Ely, R. E. García, *J. Power Sources* **2015**, *275*, 912.
[53] W. Xiao, L. Zhao, Y. Gong, J. Liu, C. Yan, *J. Membr. Sci.* **2015**, *487*, 221.
[54] A. Liu, S. Li, Z. Jiang, J. Du, Y. Tao, J. Lu, Y. Cheng, H. Wang, *J. Power Sources* **2022**, *521*, 230947.
[55] M. F. Lagadec, R. Zahn, V. Wood, *Nat. Energy* **2019**, *4*, 16.
[56] S. Huo, L. Sheng, W. Xue, L. Wang, H. Xu, H. Zhang, X. He, *InfoMat.* **2023**, *5*, e12394.
[57] S. Porporato, M. Bartoli, A. Piovano, N. Pianta, A. Tagliaferro, G. A. Elia, R. Ruffo, C. Gerbaldi, *Batteries* **2022**, *8*, 183.
[58] M. Carboni, J. Manzi, A. R. Armstrong, J. Billaud, S. Brutti, R. Younesi, *ChemElectroChem.* **2019**, *6*, 1745.
[59] T. Cai, Y. Wang, F. Zhao, Z. Ma, P. Kumar, H. Xie, C. Sun, J. Wang, Q. Li, Y. Guo, J. Ming, *Adv. Ener. Mater.* **2024**, *14*, 2400569.
[60] H. Cheng, Q. Sun, L. Li, Y. Zou, Y. Wang, T. Cai, F. Zhao, G. Liu, Z. Ma, W. Wahyudi, Q. Li, J. Ming, *ACS Energy Lett.* **2022**, *7*, 490.
[61] H. Zheng, K. Jiang, T. Abe, Z. Ogumi, *Carbon* **2006**, *44*, 203.
[62] H. Wang, L. Sheng, G. Yasin, L. Wang, H. Xu, X. He, *Energy Storage Mater.* **2020**, *33*, 188.

[63] Q. Wang, C. Zhao, X. Lv, Y. Lu, K. Lin, S. Zhang, F. Kang, Y.-S. Hu, B. Li, *J. Mater. Chem. A* **2019**, *7*, 24857.
[64] M. R. Busche, T. Drossel, T. Leichtweiss, D. A. Weber, M. Falk, M. Schneider, M.-L. Reich, H. Sommer, P. Adelhelm, J. Janek, *Nat. Chem.* **2016**, *8*, 426.
[65] J. Zheng, M. S. Kim, Z. Tu, S. Choudhury, T. Tang, L. A. Archer, *Chem. Soc. Rev.* **2020**, *49*, 2701.
[66] K. N. Wood, E. Kazyak, A. F. Chadwick, K.-H. Chen, J.-G. Zhang, K. Thornton, N. P. Dasgupta, *ACS Cent. Sci.* **2016**, *2*, 790.
[67] A. H. Willbourn, *Polymer* **1976**, *17*, 965.
[68] S. Drvarič Talian, J. Bobnar, A. R. Sinigoj, I. Humar, M. Gaberšček, *J. Phys. Chem. C* **2019**, *123*, 27997.
[69] Z. Hu, S. Zhang, S. Dong, Q. Li, G. Cui, L. Chen, *Chem. Mater.* **2018**, *30*, 4039.
[70] Z. Li, J. Huang, B. Y. Liaw, V. Metzler, J. Zhang, *J. Power Sources* **2014**, *254*, 168.
[71] J. Xu, R. D. Deshpande, J. Pan, Y.-T. Cheng, V. S. Battaglia, *J. Electrochem. Soc.* **2015**, *162*, A2026.
[72] X. Li, Q. Wang, Y. Yang, J. Kang, *International Journal of Electrical Power & Energy Systems* **2019**, *110*, 819.